Rigid Biimidazole Ancillary Ligands as an Avenue to Bright Deep Blue Cationic Iridium (III) Complexes

*Adam F. Henwood,[a] Sloane Evariste,[b,c] Alexandra M.Z. Slawin[a] and Eli Zysman-Colman[a]**

[a] EaStCHEM School of Chemistry, University of St Andrews, St Andrews, Fife, UK, KY16 9ST, Fax: +44-1334 463808; Tel: +44-1334 463826; E-mail: eli.zysman-colman@st-andrews.ac.uk;
[b] *Département de Chimie, Université de Sherbrooke, 2500 Boul. de l'Université, Sherbrooke, QC, Canada, J1K 2R1*
[c] *Current Address: Sciences Chimiques, UMR 6226 CNRS - Université de Rennes 1, Campus de Beaulieu, Rennes Cedex, France 35042*
URL: http://www.zysman-colman.com

Abstract. Herein we report the synthesis and optoelectronic characterisation of three deep blue-emitting cationic iridium complexes, of the form $[Ir(dFppy)_2(N^N)]PF_6$, bearing biimidazole-type N^N ancillary ligands (dFppyH = 2-(2,4-difluorophenyl)pyridine). Complex **1** contains the parent biimidazole, biim, while **2** contains a dimethylated analog, dMebiim, and **3** contains an *ortho*-xylyl-tethered biimidzole, *o*-Xylbiim. We explore a strategy of tethering the biimidazole in order to rigidify the complex and increase the photoluminescent quantum yield, culminating in deep blue (λ_{max}: 457 nm in MeOH at 298 K) ligand-centered emission with a very high photoluminescent quantum yield of 68% and microsecond emission lifetime. Density Functional Theory calculations elucidate the origin of such disparate excited state kinetics across this series, especially in light of virtually identical optoelectronic properties observed for these compounds.

Introduction. For many years Organic Light-Emitting Diodes (OLEDs) have been touted as the technology that will usurp conventional fluorescent tubes as the market's dominant lighting source,[1] owing to their use of environmentally benign,[2] relatively cheap emissive materials[3] and their capacity to achieve external quantum efficiencies of 100%.[4] However, in spite of these desirable features, OLEDs have struggled to attain universal marketability as the solid-state lighting (SSL) technology of choice. The emissive materials employed are incapable of effecting balanced charge injection and mobility, thus necessitating the encapsulation of low work function, air-reactive electrodes within complex multilayer compositions.[4c] Typical fabrication of such sensitive devices thus typically requires vacuum sublimation - a process which is both labor- and cost-intensive, and requires thermally stable, non-ionic materials,[5] which limits the choice of organometallic triplet harvesters that might be used.[6]

A promising alternative lighting technology to OLEDs is Light-Emitting Electrochemical Cells (LEECs). By using charged materials they confer many of the same advantages but they allow for the circumvention of the arduous vacuum sublimation process. Processing is instead carried out by solution printing, using air-stable high work function electrodes in a single- or two-layer device architecture, making large-area artificial illumination a very real possibility.[7] Two classes of emitter materials are typically employed: 1) a mixture of conjugated polymer, ion transport material and inorganic salt such as LiOTf;[8] 2) an ionic Transition Metal Complex (iTMC).[9] Of the different families of iTMCs, by far the most widely studied and exciting class of emitters for LEECs are heteroleptic cationic iridium(III) complexes, of the form $[Ir(C\hat{}N)_2(N\hat{}N)]^+$, where C^N is a monoanionic cyclometalating bis(chelate) and N^N is a neutral diimine ancillary ligand.[5]

LEECs too present their own design challenges. Issues that still require addressing for iTMC LEECs include slow turn-on times,[10] limited device stability[11] and poor colour quality.[12] In particular, few examples exist of blue-emitting LEECs,[13] which is mainly due to a shortage of deep blue, brightly emitting complexes. Blue emitters are critical both for white light emission and as a component of RGB-based pixels in displays.

Our group has thus devoted serious attention to designing cationic iridium complexes towards obtaining blue emission, combining electron-deficient C^N and electron-rich N^N ancillary ligands, with varying degrees of success.[14] There are now a few reported examples of deep blue emitting cationic iridium complexes in solution (λ_{max} < 470 nm), but significant issues still remain regarding the brightness of these emitters.[14b,15]

In surveying the literature for electron-rich diimine ligand architectures as avenues towards deep blue emitters, we found imidazole-based ligands to be promising candidates. Complexes bearing imidazole ligands have been employed in a diverse set of photophysical applications ranging from bioimaging[16] and sensing[17] to excited state proton-coupled electron transfer (PCET)[18] and solid-state lighting.[19] Of particular interest to us were iridium complexes of the form $[Ir(C^N)_2(N^N)]^+$ bearing a 1*H*,1*H*'-2,2'-biimidazole (biim) N^N ligand. As expected, the electron-rich nature of this ligand type has been shown to give a pronounced blue-shift in emission in comparison to the prototypical complex $[Ir(ppy)_2(d\textit{t}Bubpy)]^+$ (where ppyH is 2-phenylpyrdine and d*t*Bubpy is 4,4'-di-*tert*butyl-2,2'-bipyridine, λ_{max} = 581 nm in MeCN).[14c,20] For instance, Wenger and co-workers[21] reported that $[Ir(tolpy)_2(biim)]^+$, where tolpy is 2-*p*-tolylpyridinato, showed emission maxima at 484 and 514 nm in DCM while Qiu and co-workers[19b] reported a similar complex, $[Ir(ppy)_2(dMebiim)]^+$, where dMebiim is 1,1'-dimethyl-2,2'-biimidazole, that emits at 497 nm in DCM. Most notably, Kim and co-workers

[19d] recently showed that combining the biim N^N ligand with an electron-deficient C^N ligand in $[Ir(dFpmpy)_2(biim)]^+$, where dFpmpy is 2-(2',4'-difluorophenyl)-4-methylpyridine, could achieve deep blue emission with emission maxima at 456 and 484 nm in DCM. However, despite these promising examples in terms of emission energy, photoluminescence quantum yields (Φ_{PL}) remain very low (Figure **1**).

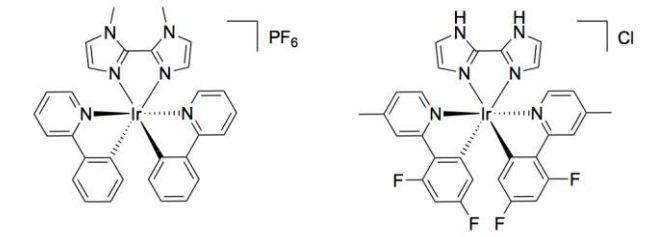

$[Ir(ppy)_2(dMebiim)]PF_6$
λ_{max}: 497 nm
Φ_{PL} = 5%
Adv. Funct. Mater., 2009, **19**, 2950

$[Ir(dFpmpy)_2(biim)]Cl$
λ_{max}: 456, 484 nm
Φ_{PL} = 10.2%
Bull. Korean Chem. Soc., 2012, **33**, 3645

Figure **1**. Literature examples of cationic iridium complexes containing a biim-based N^N ligand.

The low Φ_{PL} observed in $[Ir(ppy)_2(dMebiim)]PF_6$ was due to increased non-radiative decay kinetics, k_{nr}, where undesired twisting of the dMebiim ligand resulted from the imposed steric strain of the methyl groups. We hypothesized that in adopting a tethering strategy between the two non-coordinating biimidazole nitrogen atoms the torsional strain could be alleviated and the complex rigidified, resulting in a concomitant increase in Φ_{PL}. Four target complexes were identified (Chart **1**) to test this hypothesis. Critically, we anticipated the lack of conjugation of the tether groups in these complexes (**3** and **4**) to not adversely affect the optoelectronic properties observed for the parent compounds (**1** and **2**), with the only anticipated effect being an improvement in Φ_{PL}.

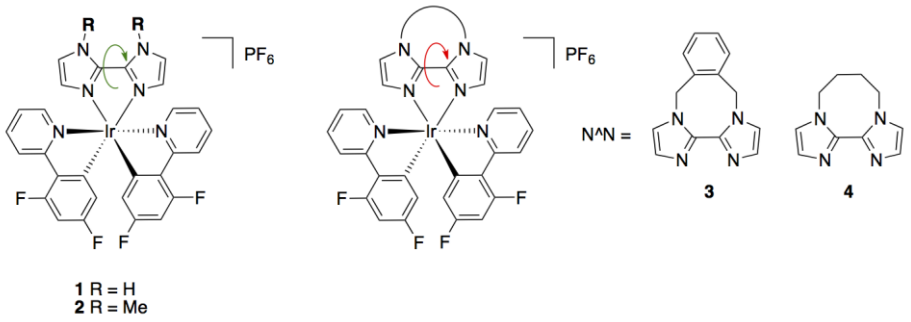

Chart **1**. Complexes under investigation in this study. The green arrow connotes a certain degree of rotational flexibility about the bond while the red arrow connotes the opposite.

Other strategies have been employed for improving Φ_{PL}, and these center around two main approaches: 1) the use of bulky groups to suppress excited state emission quenching;[19a,22] and 2) employing higher-order ter-,[15f] tetra-,[23] or even hexadentate[24] chelates as molecular rigidifiers (chelate effect). In this report, we highlight a third strategy for photoluminescence quantum yield enhancement, whereby restricting the degrees of freedom of a bidentate chelate confers increased molecular rigidity to the complex and results in higher Φ_{PL} for deep-blue emitting cationic iridium complexes. Complex **3**, in particular, has been targeted as an emitter for LEECs.

Results and Discussion

Ligand and Complex Synthesis.

The cyclometalating ligand 2-(2',4'-difluorophenyl)pyridine, dFppy, was chosen as this is the most common electron-deficient C^N ligand reported and **1** would thus serve as an appropriate benchmark complex. The dFppy ligand was prepared in good yield by a modified method to that reported previously,[25] with the corresponding μ-dichloro-bridged iridium dimer, $[Ir(dFppy)_2Cl]_2$, prepared by the method reported by Nonoyama.[26] 1*H*,1*H*'-2,2'-biimidazole, biim, was prepared in moderate yield by the condensation of glyoxal in the presence of ammonium acetate.[27] The dMebiim and *o*-Xylbiim ligands were obtained through

alkylation of biim. Alkylation of biim using methyl iodide in the presence of DMF and aqueous sodium hydroxide base at room temperature[27b] afforded dMebiim in good yield while more forcing conditions were required to obtain *o*-Xylbiim (Scheme **1**).[28] Despite repeated alkylation attempts, the butylene linked analogue ligand, Bubiim, was not able to be isolated.

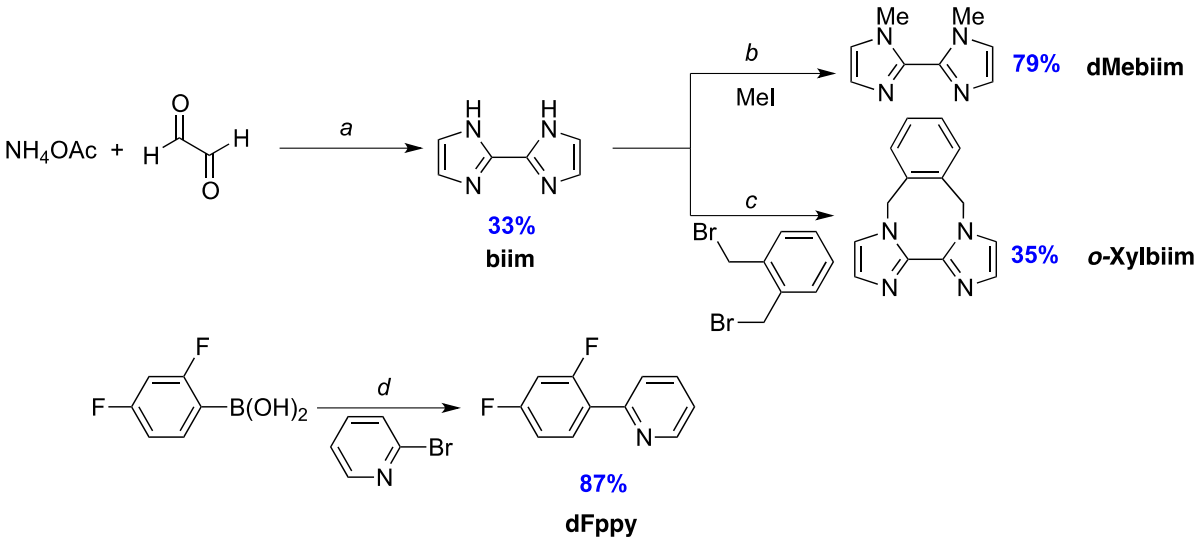

Scheme **1**. Synthesis of C^N and N^N ligands. Reagents and conditions: [a] H_2O, 40 °C, 8 h. [b] NaOH (35% w/v), DMF, RT, 12 h. [c] NaOH (35% w/v), MeCN, 82 °C, 12 h. [d] 2.0 equiv. Na_2CO_3, 5 mol% $Pd(PPh_3)_4$, N_2, 1,4-dioxane/H_2O (4:1 v/v), 105 °C, 19 h.

The iridium complexes were isolated in good yield by cleavage of $[Ir(dFppy)_2Cl]_2$ with the corresponding biimidazole in a refluxing DCM/MeOH solution followed by purification by column chromatography and isolation as the PF_6^- salt by anion metathesis with solid NH_4PF_6 (Scheme **2**). The purity and structure of the complexes were established by NMR spectroscopy, HRMS and melting point analyses. The molecular structures of **1** and **3** were determined by single-crystal X-Ray structure analysis.

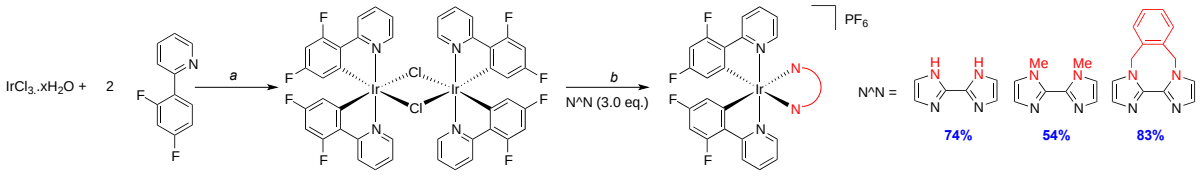

Scheme **2**. Synthesis of complexes in study. Reagents and conditions: [a] 2-$EtOC_2H_4OH/H_2O$ (4:1 v/v), 110 °C, N_2, 19 h. [b] i. CH_2Cl_2/MeOH (5:4 v/v), 55 °C, 19 h, N_2; ii. Excess solid NH_4PF_6.

X-Ray and Solution State Structural Elucidation.

Crystals of **1** and **3** were grown by vapor diffusion of Et_2O into solutions of MeCN and DCM/MeOH, respectively. The structures have been deposited with the CCDC (deposition numbers CCD 1001467-1001468). The poor quality of the dataset for **3** precludes any detailed analysis of the structural parameters though it does provide convincing proof of connectivity. Both complexes exhibit a distorted octahedral geometry (Figure **2**) with the pyridyl groups in the typical *trans* relationship. In **1** the bite angles of the C^N ligands [80.8(30)° and 81.2(4)°] and biimidazole-based N^N ligand [76.1(2)°] are comparable with those reported for cationic biimidazole complexes[21] and related bis(triazole) complexes,[14a] with the reduced bond angle of the biimidazole attributable to the smaller chelate angle of five-membered ring chelates over six-membered ring chelates.[27a] Similar bond angles to the metal are reported in other biimidazole-to-metal crystal structures such as with iron (biim = 80.39°, *o*-Xylbiim = 75.4°)[28] and with rhodium (biim = 79.24).[29] There appears to be some changes in torsion angles between **1** and **3**. In **1** the biim ligand is relatively flat whereas in **3** the $N_{(Ir)}$-C-C-$N_{(Ir)}$ torsion angle is 8°.

The packing in the crystal structures differs between **1** and **3**. In **1** there are strong hydrogen bond interactions between the fluorine atoms on the PF_6^- anion and the N-H biimidazole hydrogen atoms, [H(3)···F (1) 1.96, N(3)···F(1) 2.931(8) Å, N-H···H 170.9°; H(10) ···F(5)

1.95, N(10)···F(5) 2.889(9) Å; N(10)-H(10)···F(5) 158.6°]. This type of hydrogen-bonded ion pairing interaction has been previously observed with Wenger's[21] $[Ir(tolpy)_2(biim)]^+$ complex, which crystallized in the presence of the 3,5-dinitrobenzoate anion, as well as with $[Ir(pqx)_2(biim)]Cl$ (pqx = phenylquinoxaline), where the chloride anion hydrogen bonds with the distal NH groups of the biim.[19c]

Solution state NMR spectroscopy suggests that complex **3** exists as at least two sets of diastereomeric atropisomers (*vide infra*). However, in the solid **3** crystallises as a racemate in the *P*-1 space group. The absence of biimidazole hydrogen atoms precludes similar interactions to those seen in **1.** There is a weak interaction from a fluorine atom of the dFppy to an *o*-xylyl aryl hydrogen atom [H(50)···F(29) 2.35, C(50)···F(29) 3.29(3) Å; C(50)-H(50)···F(29) 170.2°]. Interactions with the PF_6^- anion in this instance are minimal.

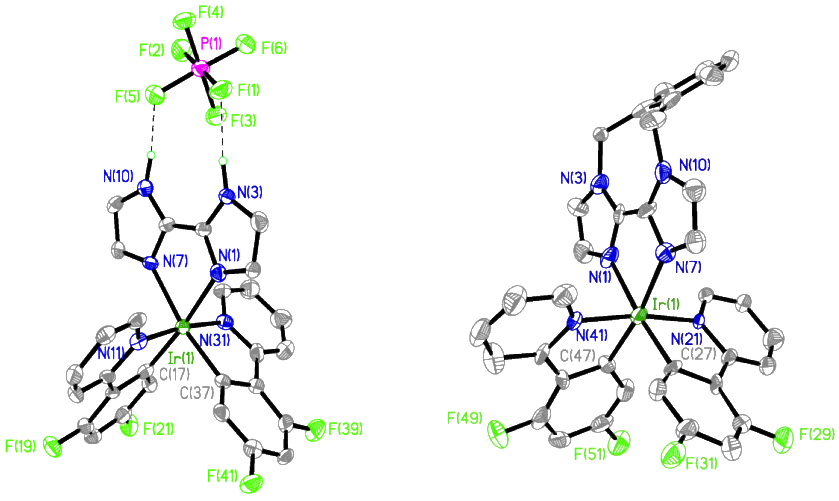

Figure **2**. Molecular structures of **1** (left) and **3** (right) with 50% probability ellipsoids. The majority of the hydrogen atoms and the counterion in **3** have been omitted for clarity. Selected bond lengths (Å) and angles (°) for **1**: Ir(1)-N(1) 2.158(8), Ir(1)-N(7) 2.173(6), Ir(1)-N(11) 2.027(8), Ir(1)-N(3)1 2.038(8), Ir(1)- C(1)7 2.019(10), Ir(1) –C(3)7 2.033(8), N(1)-Ir(1)-N(7) 76.1(2), N(11)-Ir(1)-C(17) 81.2(4), N(31)-Ir(1)-C(37) 80.8(3).

Characterization of complex **3** by solution ^{1}H NMR proved challenging owing to the generally poor solubility in virtually all solvents and its surprisingly complex ^{1}H NMR spectrum, especially when compared with the ^{1}H NMR spectra of complexes **1** and **2** (Figure **3**).

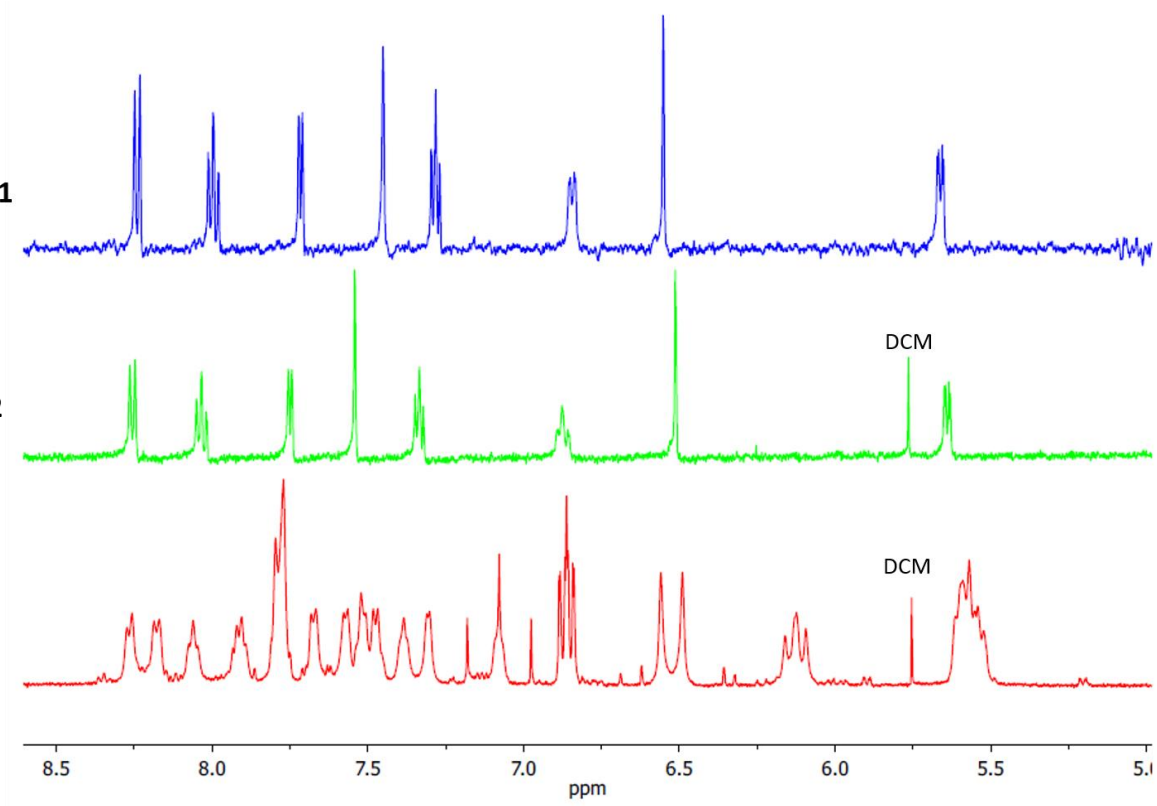

Figure **3**. Stacked plot of ^{1}H NMR spectra of complexes **1**, **2** and **3** at room temperature in DMSO-d_6.

The complexity of this spectrum at room temperature was attributed to slow fluxional motion of the *o*-xylyl group resulting in the detection of two or more diastereomeric atropisomers at this temperature (Figure **4**). Upon heating, the ^{1}H NMR spectrum simplifies to the expected pattern. For instance, at 318 K, there is an observed coalescence of the doublet at 6.55 ppm. Eyring analysis of this coalescence phenomenon suggests the activation barrier to *o*-xylyl ring flipping is 82.97 kJ mol^{-1}.[30]

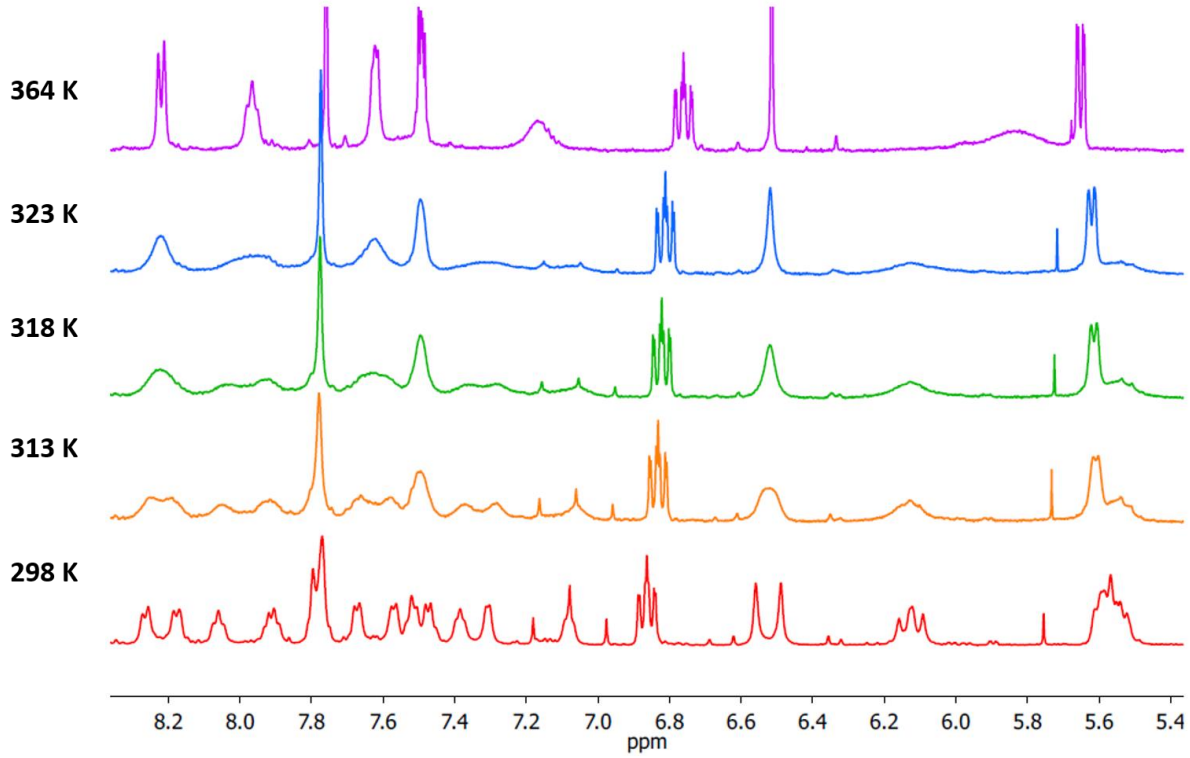

Figure **4**. Variable temperature ^{1}H NMR study of **3** in DMSO-d_6.

Cyclic voltammetry.

The electrochemical behavior of complexes **1**–**3** was investigated by cyclic voltammetry (CV) in deaerated MeCN solution containing *n*-NBu_4PF_6 as the supporting electrolyte and using Fc/Fc^+ as an internal standard at 298 K. All potentials are referenced with respect to SCE (Fc/Fc^+ = 0.38 V in MeCN)[31] and all reported data were carried out at a scan rate of 50 mV s^{-1}. The HOMO energy levels were determined from the relation $E_{HOMO} = -[E^{ox}_{pa\ vs\ Fc/Fc+} + 5.39]$ eV,[32] while the lack of a detectable reduction wave in the accessible solvent window necessitated estimating the E_{LUMO} energies from the sum of the E_{HOMO} values and the optical band gap values, $E_{0,0}$, for each complex. $E_{0,0}$ was inferred from the intersection point between the absorption and emission spectra obtained at 298 K in MeOH. Table **1** summarizes the relevant electrochemical data.

Table **1**. Electrochemical data and orbital energies for **1**-**3**.[a]

Compound	$E^{ox}_{1/2}$ (V)	ΔE_p (mV)	E_{HOMO}(eV)[b]	E_{LUMO}(eV)[c]	$E_{0,0}$ (eV)[d]
1	1.51	76	-6.56	-3.71	2.85
2	1.45	79	-6.50	-3.64	2.86
3	1.44	72	-6.49	-3.59	2.90

[a] All measurements were performed at 50 mV s^{-1} in deaerated MeCN solution using Fc/Fc^+ as an internal standard, and are referenced with respect to SCE (Fc/Fc^+ = 0.38 V in MeCN).[31] [b] $E_{HOMO} = -[E^{ox}_{pa\ vs\ Fc/Fc+} + 5.39]$ eV.[32] [c] $E_{LUMO} = E_{HOMO} + E_{0,0}$ eV. [d] $E_{0,0}$ estimated from the intersection point of the absorption and emission spectra at 298 K in MeOH.

The oxidation potentials of **1-3** are expectedly virtually unchanged across the series, with each complex demonstrating a single, quasi-reversible oxidation wave in the region of 1.5 V. These oxidation potentials are very similar to that previously reported[14c] for $[Ir(dFMeppy)_2(bpy)]PF_6$ (dFMeppy is 2-(2',4'-difluorophenyl)-4-methylpyridine and bpy is 2,2'-bipyridine), where $E^{ox}_{1/2}$ = 1.55 V under similar conditions. The oxidation is thus assigned to the Ir^{III}/Ir^{IV} redox couple with contribution from the C^N ligands. DFT calculations (*vide infra*) corroborate this analysis. Surprisingly, despite virtually identical photophysical properties to **1**, the electrochemical properties of Kim's[19d] $[Ir(dFpmpy)_2(biim)]^+$ complex differ somewhat to our own, with a reported $E^{ox}_{1/2}$ value of 1.59 V versus Fc/Fc^+ in DCM, resulting in modestly higher reported E_{HOMO} (-6.25 eV) and E_{LUMO} (-3.56 eV) energies. The HOMO-LUMO energy gap, estimated from the optical gap ($E_{0,0}$), is however similar (2.69 eV) to those in this study.

Solution state photophysical behavior.

A comprehensive summary of the relevant photophysical data undertaken in this study is given in Table **2**; absorptivity data may be found in the electronic supporting information (ESI), Table **S1**. Figure **4** shows the normalized absorption and emission spectra for complexes **1** - **3** at room temperature in MeOH, also shows the normalized 77 K emission spectra in a 1:1 MeOH/EtOH glass. The absorption spectra for the complexes are relatively

unstructured, typical for iridium-biimidazole complexes,[19b,19d] with the intense band at around 250 nm region assigned to spin-allowed ligand centered (^{1}LC) $^1\pi\rightarrow\pi^*$ transitions. All three complexes also demonstrate a distinct lower energy absorption band at about 370 nm, as well as a small tail into the near UV region. These bands are also present in $[Ir(dFpmpy)_2(biim)]^+$ and were attributed by Kim to be comprised of a mix of $^3\pi\rightarrow\pi^*$ and spin-allowed and spin-forbidden metal-to-ligand charge transfer (^{1}MLCT) and (^{3}MLCT) transitions.[19d] Alkylation of the biim ligand leads to a more structured absorption profile, particularly between 250-370 nm. Excitation spectra for **1-3** (Figures **S16-S18**) reproduce these characteristic features.

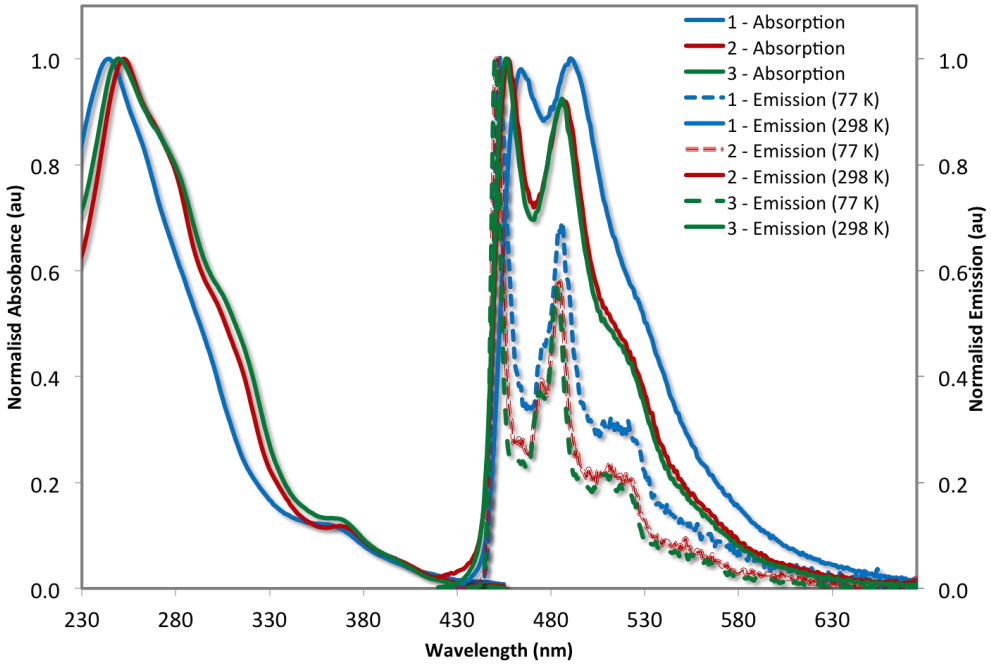

Figure **4**. Normalized absorption spectra of **1-3** in aerated MeOH at 298 K and normalized emission spectra in deaerated MeOH at 298 K and 1:1 MeOH:EtOH glass at 77 K.

The structured emission profiles at 77 K and 298 K arise from a ^{3}LC emission (Figure **4)**. The absence of any rigidochromic shift in the emission maxima further corroborates the ^{3}LC nature of the emission. At both 298 and 77 K, two high-energy emission maxima are observed at around 455 nm and 484 nm, along with lower vibronic emission peaks tailing out to about 650 nm. The near identical emission spectra across the three complexes verifies our

assertion that the electronics across the series are unchanging, with only a slight blue shift in emission arising from incorporating the alkyl groups in place of the parent protons.

Table **2**. Relevant photophysical data for **1**-**3**.[a]

	λ_{em} (nm)[b]		Φ_{PL} (%)[c]	τ_e		k_r	k_{nr}
	77 K	298 K	298 K	77 K(μs)	298 K (ns)	(x10^5 s^{-1})	(x10^5 s^{-1})
1	453, 486	464, 490	20	3.682	1559	1.28	5.13
2	451, 484	457, 486	2	3.718	91	2.20	107.69
3	450, 483	457, 487	68	3.956	3840	1.77	0.83

[a] 298 K measurements in deaerated MeOH and 77 K measurements in 1:1 MeOH/EtOH glass. [b] Principal emission peaks listed. [c] Quinine sulfate used as the reference (Φ_{PL} = 54.6% in 0.5 M H_2SO_4 at 298 K).[33]

Though the Stokes shifts for **1-3** are very small, the presence of iridium and the microsecond emission lifetimes point to a phosphorescence emission. Low temperature emission lifetimes (τ_e) of all three complexes in 1:1 MeOH/EtOH glass are similar and are in the range of 3.6 – 4.0 μs. However, at 298 K while τ_e for **1** and **3** remains in the microsecond regime, that for **2** drops significantly to 90 ns, indicative of substantial contributions to k_{nr} for this complex at room temperature. The photoluminescence quantum yield, Φ_{PL}, for **1** is 20% and decreases markedly for **2** to only 2%. Gratifyingly, the Φ_{PL} for **3** is a remarkable 68%! These figures are reflected in the excited state kinetics. While the radiative rate constants, k_r, are similar for **1-3** (ranging from 1.3 to 2.2 × 10^5 s^{-1}), k_{nr} values differ dramatically across the series. Complex **2** has a k_{nr} of 107 × 10^5 s^{-1}, which is two orders of magnitude larger than that calculated for **1** at 5.1 × 10^5 s^{-1}. The brightest complex, **3**, has a calculated k_{nr} of 0.8 × 10^5 s^{-1}, which is six-fold smaller than that of **1**.

Theoretical Calculations.

A combined density functional theory (DFT) and time-dependent DFT (TDDFT) study was undertaken to rationalize the optoelectronic properties and to verify the hypothesis that tethering in this instance leads to a less strained geometry.[34] Complexes **1-3** and butyl tethered analog **4** were modeled using Gaussian 09[35] using the following DFT protocol at the B3LYP[36] level of theory with the SBKJC-DVZ[37] basis set for iridium, 6-31G* for heavy atoms directly coordinated to iridium and 3-21G* for all other atoms[37a,38] in the presence of the solvent MeCN.[39]

Table **3**. Selected calculated average structural parameters for **1-4**.[a]

Complexes	**1**		**2**		**3**		**4**	
	S_0	T_1	S_0	T_1	S_0	T_1	S_0	T_1
Ir-N_{N^N}	2.1966	2.2138	2.1702	2.1902	2.1820	2.1936	2.0188	2.2006
Ir-N_{C^N}	2.0737	2.0650	2.0733	2.0635	2.0736	2.0653	2.0756	2.0668
Ir-C_{C^N}	2.0198	2.0072	2.0228	2.0086	2.0213	2.0087	2.0209	2.0081
N_{N^N}-Ir-N_{N^N}	75.4	75.1	74.3	74.3	74.9	74.5	75.1	74.8
N_{C^N}-Ir-N_{C^N}	80.4	81.2	80.4	81.3	80.4	81.2	80.4	81.1
$(N\text{-}C\text{-}C\text{-}N)_{N^N}$	0.1	1.6	3.1	11.5	1.4	1.5	8.7	9.2

[a.] Bond lengths in Å and bond angles in °. C^N = dFppy.

The geometry of the ground state structures was fully optimized without the imposition of symmetry restrictions. Each complex adopts a pseudo-octahedral geometry. Selected structural parameters for **1-4** are summarized in Table **3**. Computed geometries for **1** and **3** generally reproduce those found in the crystal structure though the Ir-N_{N^N} and Ir-N_{dFppy} bonds for **1** and **3** are predicted to be slightly elongated by around 0.02 Å while there is a slightly more pronounced torsion between the two imidazole fragments in the crystal structure of **3** of 8°. The geometries of the triplet state were optimized using spin-unrestricted

DFT calculations at the UB3LYP level. In the triplet state, the Ir-N_{N^N} is predicted to be slightly elongated while modest bond length contractions are predicted between the iridium center and the dFppy ligands. Structural differences manifest most markedly in the (N-C-C-N)$_{N^N}$ dihedral angle. There is a large change in the (N-C-C-N)$_{N^N}$ torsion observed in **2** between the S_0 and T_1 states while in **4**, a larger twist is predicted compared to **1-3**. This results from a conformational compensation in this dihedral angle in order to minimize repulsive interactions in the pseudo-gauche conformation of the butyl linker (47.2^o). Complex **3** exhibits the most rigid conformation.

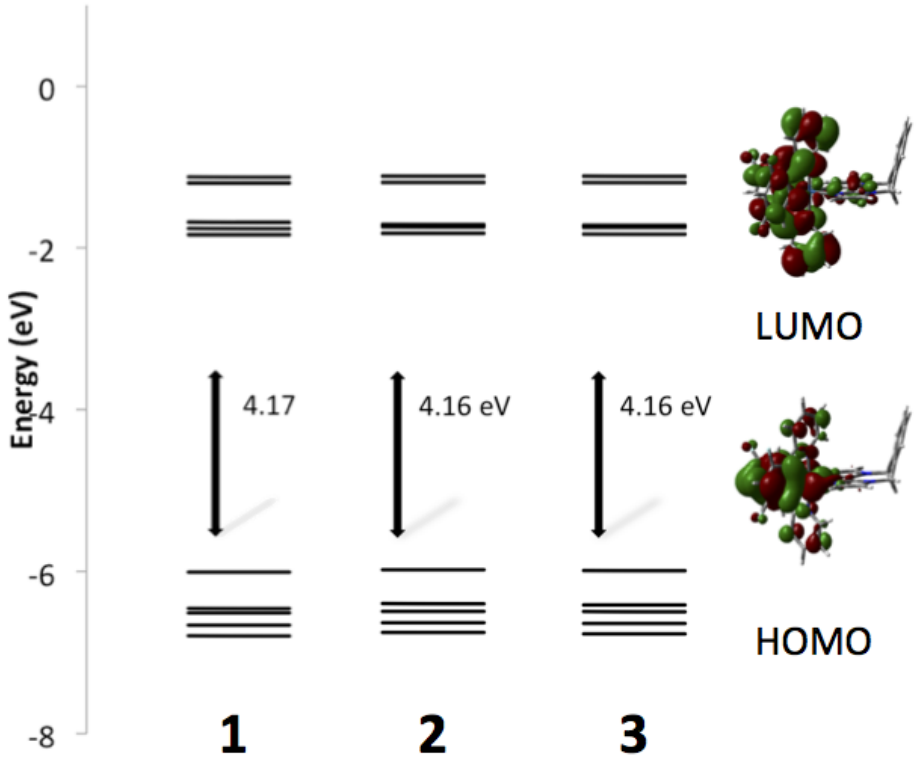

Figure **5**. Calculated energy level scheme for the Kohn-Sham orbitals between HOMO-4 to LUMO+4 of **1-3**, and the associated DFT calculated HOMO-LUMO energy gap (in eV). Electron density contour plots for **3** (0.002 e bohr^{-3}). The contour plots for **1** and **2** mirror those of **3**.

Figure **5** show a comparison of the relative energies of the five highest energy occupied and five lowest energy unoccupied molecular orbitals (MOs) for **1-3**. The HOMO is localized on both the aryl ring of the C^N ligands and the iridium atom (t_{2g}). The LUMO is also situated on the dFppy ligands though there is now increased contribution from the pyridine moiety. The large HOMO-LUMO gap for all three is calculated to be ca. 4.16 eV. The effect of alkylation of the biim ligand does not significantly perturb the energies of the frontier molecular orbitals.

The computations reproduce the principal features in the UV-Visible spectra for the complexes (cf. Figures **S19-S21**). TDDFT analysis for **1-3** predicts a T_1 state that contains two major contributions: HOMO⦿LUMO (51%) and HOMO-2⦿LUMO+1 (22%). The qualitative description of the triplet state that results is predominantly ligand-centered (^{3}LC) on the dFppy ligands with some metal-to-ligand charge transfer (^{3}MLCT) from the iridium t_{2g} orbitals to the dFppy ligands. The spin densities for the T_1 state for **1-4** are shown in Figure **6** and all show similar topologies with the spin density localized on one of the two dFppy ligands, implying an emission resulting from a ^{3}LC state. This assignment is consistent the observed structured emission at 298 K in MeOH.

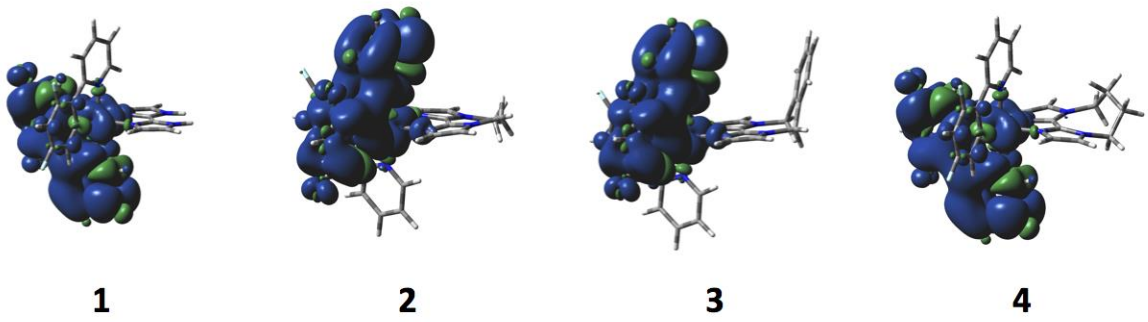

Figure **6**. Calculated spin density contours of the T_1 state for **1-4** (isocontour value of 0.0004 au).

The emission energy was predicted using two different methodologies. The phosphorescence is estimated as the difference between the T_1 and S_0 states in their respective optimized geometries ($E_{0,0}$), which is a good indicator of the $E_{0,0}$ emission measured at 77 K. For **1-3**, an emission at 430 nm was predicted. The λ_{max} at 77 K ranged from 451-453 nm. The adiabatic electronic emission (E_{AE}) is determined from the vertical energy difference between the T_1 and S_0 states at the optimized geometry of the T_1 state. For **1-3**, an emission at 487 nm was predicted. The λ_{max} at 298 K ranged from 457-464 nm. The calculations reproduce (E_{AE}) quite accurately the solution state emission observed at 298 K, with relative errors of about 6%.

Conclusions.

In summary, three new cationic iridium(III) complexes bearing biimidazole-type ancillary ligands have been reported. By exploring the role of alkylation of the biimidazole, we have dramatically modified the excited state kinetics of these three complexes without any significant changes to the electronics of these deep blue emitters, which all emit in the deep blue at around 455 nm in MeOH solution. Crucially, we have reported a dramatic increase in the photoluminescence quantum yield for complex **3** of 68% compared to 2% for **2** – among the very brightest of deep blue (λ_{max} < 470 nm) cationic iridium emitters reported in the literature. Microsecond emission lifetimes in **3** were maintained. However, poor solubility of these compounds has hindered their subsequent device fabrication. Current efforts are underway to make **3** more soluble and thus processable as an emissive layer in a LEEC and results thereof will be reported in due course.

Acknowledgements. EZ-C acknowledges the University of St Andrews for financial support.

Experimental Section

General Synthetic Procedures. Commercial chemicals were used as supplied. All reactions were performed using standard Schlenk techniques under inert (N_2) atmosphere with reagent grade solvents. Flash column chromatography was performed using silica gel (Silia-P from Silicycle, 60 Å, 40-63 μm). Analytical thin layer chromatography (TLC) was performed with silica plates with aluminum backings (250 μm with indicator F-254). Compounds were visualized under UV light. ^{1}H, ^{13}C and ^{19}F NMR spectra were recorded on a Bruker Avance spectrometer at 500 MHz, 126 MHz and 471 MHz respectively. The following abbreviations have been used for multiplicity assignments: "s" for singlet, "d" for doublet, "t" for triplet, "m" for multiplet and "br" for broad. Deuterated chloroform ($CDCl_3$) and deuterated DMSO (DMSO-d_6) were used as the solvents of record. Melting points (Mp's) were recorded using open-ended capillaries on an Electrothermal melting point apparatus and are uncorrected. High-resolution mass spectra were recorded on a quadrupole time-of-flight (ESI-Q-TOF), model ABSciex 5600 Triple TOF in positive electrospray ionization mode and spectra were recorded using sodium formate solution as calibrant. The iridium(III) dimer, $[(dFppy)_2Ir(\mu\text{-}Cl)]_2$ was prepared according to the procedure described by Nonoyama.[26]

Ligand Syntheses.

2-(2,4-Difluorophenyl)pyridine (dFppy). The synthesis of this ligand is by a modified method to a previously reported method.[40] 2,4-Difluorophenylboronic acid (1.1 equiv.), 2-bromopyridine (1.0 equiv.), sodium carbonate (2.0 equiv.) were added to a Schlenk tube containing a mixture of 1,4-dioxane and distilled water (4:1 v/v) to obtain a concentration of 0.15 to 0.20 M. The reaction mixture was degassed via three freeze-pump-thaw cycles. Upon warming to room temperature from the third cycle, $Pd(PPh_3)_4$ (5 mol%) was added to the tube under positive nitrogen pressure and the tube was sealed. The mixture was refluxed for 19 h

and then cooled to room temperature. The mixture was poured onto distilled water and extracted multiple times with dichloromethane. The organic fractions were combined, washed with a portion of brine and dried over magnesium sulfate. Filtration and evaporation under reduced pressure gave the crude product (1.45 g). The crude product was purified by flash column chromatography (silica, hexane/ethyl acetate gradient 100:0 to 80:20) to give 1.31 g of pure compound as a colourless oil. **Yield:** 87%. **R_f:** 0.48 (20% EtOAc/hexanes on silica). **^{1}H NMR (500 MHz, $CDCl_3$) δ (ppm):** 8.72 (dt, *J* = 4.5, 1.0 Hz, 1H), 8.03 - 7.99 (m, 1H), 7.75 (d, *J* = 4.0 Hz, 2H), 7.28 – 7.23 (m, 1H), 7.03 – 6.99 (m, 1H), 6.93 – 6.90 (m, 1H). **^{13}C NMR (126 MHz, $CDCl_3$) δ (ppm):** 164.6, 162.1, 159.5, 152.7, 149.9, 136.6, 132.3, 124.4, 122.6, 112.1, 104.5. **^{19}F {^{1}H} NMR (471 MHz, $CDCl_3$) δ (ppm):** -109.3 (d, *J* = 6.8 Hz, 1F), -113.0 (d, *J* = 6.8 Hz, 1F). **GCMS:** (13.6 min) $[M]^+$: 191. The characterisation matches that reported.[40]

1*H*,1'*H*-2,2-biimidazole (biim): Synthesis of this ligand was as outlined in the literature.[41] To a mixture of ammonium acetate (2.7 equiv.) in distilled water at 40 °C was added dropwise 40% aqueous glyoxal solution (1.0 equiv.) over a period of 3 h to give a concentration of .01 M. The mixture was allowed to stir for a further 5 h at room temperature. The reaction mixture was filtered and washed multiple times with distilled water and acetone to give 8.31 g of a brown crude product. This material was added to ethylene glycol (0.5 M), heated to 150 °C and treated with decolourising carbon. Filtration saw product precipitate immediately, with further washings with distilled water to maximise product precipitation. The product was filtered and dried to give 2.47 g as a cream white powder. **Yield:** 33%. **R_f:** 0.12 (10% MeOH/DCM on silica). **Mp:** 350 - 352 °C. **Litt:** > 300 °C.[27a] **^{1}H NMR (500 MHz, DMSO-d_6) δ (ppm):** 12.67 (s, 2H), 7.14 (s, 2H), 7.00 (s, 2H). **^{13}C NMR (126 MHz,**

$CDCl_3$) δ (ppm): 139.8, 128.7, 117.9. The ^{1}H NMR differs from that previously reported but matches that determined by us from a commercial source.[27a]

1,1'-Dimethyl-2,2'-biimidazole (dMebiim): Synthesis of this ligand was as outlined in the literature.[41] 1*H*,1'*H*-biimidazole (l.0 equiv.) was added to a mixture of aqueous sodium hydroxide (5.6 equiv., 35% w/v) in DMF to give a concentration of 0.9 M. This was stirred for 1 h. The mixture turned green and then black over the course of the hour. Methyl iodide (3.0 equiv.) was then added slowly to the reaction mixture. The mixture was left to stir for 19 h at room temperature. The crude reaction mixture was then poured onto distilled water and extracted with chloroform multiple times. The combined organic layers were washed with water and dried over sodium sulfate. Filtration and evaporation under reduced pressure gave the crude product (0.29 g). Purification by flash column chromatography (silica, dichloromethane/ethanol gradient 100:0 to 95:5) afforded 0.19 g of the product as an off-white solid. **Yield:** 79%. **R_f:** 0.25 (10% EtOAc/hexanes on silica). **Mp:** 117 - 118 °C. **^{1}H NMR (500 MHz, $CDCl_3$) δ (ppm):** 7.11 (s, 2H), 6.96 (s, 2H), 4.04 (s, 6H). **^{13}C NMR (126 MHz, $CDCl_3$) δ (ppm):** 128.0, 122.8, 35.5. Characterisation matches that previously reported, although we only detected three ^{13}C resonances.[41]

1,1'-(α,α'-*o*-Xylylene)-2,2-biimidazole (*o*-Xylbiim): Synthesis of this ligand was as outlined in the literature.[28] To a solution containing α,α'-dibromo-*o*-xylene (1.0 equiv.) in acetonitrile (0.1 M) was added with stirring 1*H*,1'*H*-biimidazole (1.2 equiv.) followed by aqueous sodium hydroxide (5.6 equiv., 35% v/w) solution. The temperature was increased to reflux, where after about 10 min a yellow-brown solution formed. The mixture was maintained at reflux overnight, before being cooled to room temperature. After addition of distilled water the mixture was extracted with multiple times with dichloromethane. The organic fractions were

combined, dried over anhydrous magnesium sulfate and then evaporated to dryness under reduced pressure. The crude product was washed with portions of diethyl ether, affording 0.23 g of the pure compound as an off-white solid. **Yield:** 35%. **Mp:** 288 - 291 °C. **Litt:** 284 - 292 °C.[27a] **^{1}H NMR (500 MHz, DMSO-*d*$_6$) δ (ppm):** 7.47 (d, *J* = 1.0 Hz, 2H), 7.41 - 7.47 (m, 4H), 7.11 (d, *J* = 0.5 Hz, 2H), 4.97 (s, 4H). **^{13}C NMR (126 MHz, CDCl$_3$) δ (ppm):** 139.4, 133.9, 130.1, 128.9, 128.7, 122.1, 49.0. Characterisation matches that previously reported.[27a]

General procedure for the synthesis of [(C^N)$_2$Ir(N^N)]PF$_6$ complexes. To a Schlenk tube containing [Ir(dFppy)$_2$Cl]$_2$ (1.0 equiv.) and N^N ligand (3.0 equiv.) were added DCM and MeOH (5:4 v/v) to give a concentration of 0.03 M. The mixture was degassed via three freeze-pump-thaw cycles, before backfilling with N_2 upon thawing from the third cycle. The reaction mixture was heated to 55 °C for 19 h. Over the course of the reaction the mixture darkened in colour. The solution was cooled to room temperature and solid NH_4PF_6 (10.0 equiv.) was added and the reaction mixture was left to stir for a further 1 h. The resulting suspension was evaporated to dryness, with the residue then copiously washed with Et_2O and distilled water. This crude product was purified by flash column chromatography (silica, DCM/MeOH gradient 100:0 to 95:5). Fractions containing the desired complex were combined and solid NH_4PF_6 (10 equiv.) was added. The suspension was stirred at room temperature for 0.5 h. This mixture was then evaporated to dryness, washed vigorously with distilled water and dried to afford the pure material.

Iridium (III) bis[2-(4',6'-difluorophenyl)-pyridinato-N,C$^{2'}$]-*N*,*N*'-(1*H*,1'*H*-2,2'-biimidazole) hexafluorophosphate: [(dFppy)$_2$Ir(biim)](PF$_6$), 1: yellow powder (0.094 g). **Yield**: 74%. **Mp:** 310 – 311 °C. **^{1}H {^{19}F} NMR (500 MHz, DMSO-*d*$_6$) δ (ppm):** 8.24 (d,

J = 8.5 Hz, 2H), 8.0 (td, *J* = 1.5, 7.8 Hz, 2H), 7.72 (d, *J* = 5.5 Hz, 2H), 7.45 (s, 2H), 7.28 (td, *J* = 1.0, 7.0 Hz, 2H), 6.84 (dd, *J* = 2.0, 8.8 Hz, 2H), 6.55 (d, *J* = 1.0 Hz, 2H), 5.66 (dd, *J* = 2.5, 8.0 Hz, 2H). **^{19}F {^{1}H} NMR (471 MHz, DMSO-*d*$_6$) δ (ppm):** -70.09 (d, *J* = 712.2 Hz, 6F), -107.72 (d, *J* = 9.42 Hz, 2F), -109.7 (d, *J* = 9.89 Hz, 2F)**. HR-MS (**ES-Q-TOF**): [M-PF$_6$]$^+$ Calculated:** ($C_{28}H_{18}N_6F_4Ir$) 707.1158; **Found:** 707.1130.

Iridium (III) bis[2-(4',6'-difluorophenyl)-pyridinato-N,C$^{2'}$]-*N,N'*-(1,1'-dimethyl-2,2'-biimidazole) hexafluorophosphate: [(dFppy)$_2$Ir(dMebiim)](PF$_6$), 2: yellow powder (0.062 g). **Yield**: 54%. **Mp:** 325 – 326 °C. **^{1}H {^{19}F} NMR (500 MHz, 364 K, DMSO-*d*$_6$) δ (ppm):** 8.25 (d, *J* = 7.5 Hz, 2H), 8.03 (t, *J* = 7.8 Hz, 2H), 7.74 (d, *J* = 6.0 Hz, 2H), 7.53 (d, *J* = 1.5 Hz, 2H), 7.33 (td, *J* = 1.0, 6.5 Hz, 2H), 6.87 (t, *J* = 6.0 Hz, 2H) 6.50 (d, *J* = 1.5 Hz, 2H), 5.63 (dd, *J* = 2.5, 8.0 Hz, 2H) 4.22 (s, 6H). **^{19}F {^{1}H} NMR (471 MHz, DMSO-*d*$_6$) δ (ppm):** -70.14 (d, *J* = 712.2 Hz, 6F), -107.75 (d, *J* = 9.9, 2F), -109.77 (d, *J* = 9.9, 2F)**. HR-MS (**ES-Q-TOF**): [M-PF$_6$]$^+$ Calculated:** ($C_{30}H_{22}N_6F_4Ir$) 735.1471; **Found:** 735.1442.

Iridium (III) bis[2-(4',6'-difluorophenyl)-pyridinato-N,C$^{2'}$]-*N,N'*-1,1'-(α,α'-*o*-Xylylene)-2,2-biimidazole hexafluorophosphate: [(dFppy)$_2$Ir(Xylbiim)](PF$_6$), 3: yellow powder (0.062 g). **Yield**: 83%. **Mp:** 359 – 360 °C. **^{1}H {^{19}F} NMR (500 MHz, DMSO-*d*$_6$) δ (ppm):** 8.22 (d, *J* = 8.0 Hz, 2H), 7.97 (t, *J* = 7.5 Hz, 2H), 7.76 (d, *J* = 1.0 Hz, 2H), 7.69 – 7.57 (m, 3H), 7.56 – 7.46 (m, 3H), 7.17 (s, br, 2H), 6.79 – 6.73 (m, 2H), 6.51 (d, *J* = 1.0 Hz, 2H), 5.86 (s, br, 4H), 5.65 (dd, *J* = 2.0, 8.8 Hz, 2H). **^{19}F {^{1}H} NMR (471 MHz, DMSO-*d*$_6$) δ (ppm):** 70.13 (d, *J* = 712.2 Hz, 6F), -107.60 (m, 2F), -109.7 (m, 2F)**. HR-MS (**ES-Q-TOF**): [M-PF$_6$]$^+$ Calculated:** ($C_{36}H_{24}N_6F_4Ir$) 809.1628; **Found:** 809.1597.

Photophysical measurements. All samples were prepared in HPLC grade methanol with varying concentrations on the order of μM. Absorption spectra were recorded at RT using a Shimadzu UV-1800 double beam spectrophotometer. Molar absorptivity determination was verified by linear least-squares fit of values obtained from at least three independent solutions at varying concentrations with absorbance ranging from 1.26×10^{-4} to 3.43×10^{-5} M.

The sample solutions for the emission spectra were prepared in HPLC grade MeOH and degassed via three freeze-pump-thaw cycles. Steady state emission and excitation spectra and time-resolved emission spectra were recorded at 298 K and 77 K using an Edinburgh Instruments F980. All samples for steady state measurements were excited at 360 nm while samples for time-resolved measurements were excited at 378 nm. Emission quantum yields were determined using the optically dilute method.[42] A stock solution with absorbance of ca. 0.5 was prepared and then four dilutions were prepared with dilution factors of 5, 6.6, 10 and 20 to obtain solutions with absorbances of ca. 0.1 0.075, 0.05 and 0.025, respectively. The Beer-Lambert law was found to be linear at the concentrations of the solutions. The emission spectra were then measured after the solutions were rigorously degassed via three freeze-pump-thaw cycles prior to spectrum acquisition. For each sample, linearity between absorption and emission intensity was verified through linear regression analysis and additional measurements were acquired until the Pearson regression factor (R^2) for the linear fit of the data set surpassed 0.9. Individual relative quantum yield values were calculated for each solution and the values reported represent the slope value. The equation $\Phi s = \Phi_r(A_r/A_s)(I_s/I_r)(n_s/n_r)_2$ was used to calculate the relative quantum yield of each of the sample, where Φ_r is the absolute quantum yield of the reference, n is the refractive index of the solvent, A is the absorbance at the excitation wavelength, and I is the integrated area under the corrected emission curve. The subscripts s and r refer to the sample and reference,

respectively. A solution of quinine sulfate in 0.5 M H_2SO_4 (Φ_r = 54.6%) was used as the external reference.[33]

Electrochemistry measurements. Cyclic voltammetry (CV) measurements were performed on an Electrochemical Analyzer potentiostat model 600D from CH Instruments. Solutions for cyclic voltammetry were prepared in ACN and degassed with ACN-saturated nitrogen bubbling for about 10 min prior to scanning. Tetra(*n*-butyl)ammoniumhexafluorophosphate ($TBAPF_6$; ca. 0.1 M in ACN) was used as the supporting electrolyte. An Ag/Ag^+ electrode (silver wire in a solution of 0.1 M KCl in H_2O) was used as the pseudoreference electrode; a Pt electrode was used for the working electrode and a Pt electrode was used as the counter electrode. The redox potentials are reported relative to a saturated calomel electrode (SCE) electrode with a ferrocenium/ferrocene (Fc^+/Fc) redox couple as an internal reference (0.38 V vs SCE).[31]

Density Functional Theory (DFT) Calculations. All calculations were performed with the Gaussian 09[43] suite. The level of theory for all DFT[34c,44] and TD-DFT[34d-f] calculations was B3LYP; excited-state triplet geometries were calculated using the unrestricted B3LYP method (UB3LYP).[36b,36c,45] The 6-31G* basis set[46] was used for C, H and N directly linked to Iridium while the other C, H, N and F atoms where undertaken with 3-21G* basis set,[37a,38a-e] and the VDZ (valence double ζ) with SBKJC effective core potential basis set[37] was used for Iridium. The predicted phosphorescence wavelengths were obtained by energy difference between the Triplet and Singlet states at their respective optimized geometries.[47] The energy, oscillator strength and related MO contributions for the 100 lowest singlet-singlet and 5 lowest singlet-triplet excitations were obtained from the TD-DFT/Singlets and the TD-

DFT/Triplets output files, respectively. The calculated absorption spectra were visualized with GaussSum 2.1 (fwhm: 1000 cm^{-1}).[48]

References

(1) Reineke, S.; Lindner, F.; Schwartz, G.; Seidler, N.; Walzer, K.; Lussem, B.; Leo, K. *Nature* **2009**, *459*, 234.
(2) Sasabe, H.; Kido, J. *Eur. J. Org. Chem.* **2013**, *2013*, 7653.
(3) Humphreys, C. J. *MRS Bull.* **2008**, *33*, 459.
(4) (a) So, F.; Kido, J.; Burrows, P. *MRS Bull.* **2008**, 663; (b) Tao, Y.; Yang, C.; Qin, J. *Chem Soc Rev* **2011**, *40*, 2943; (c) Slinker, J. D.; Rivnay, J.; Moskowitz, J. S.; Parker, J. B.; Bernhard, S.; Abruña, H. D.; Malliaras, G. G. *J. Mater. Chem.* **2007**, *17*, 2976.
(5) Costa, R. D.; Ortí, E.; Bolink, H. J.; Monti, F.; Accorsi, G.; Armaroli, N. *Angew. Chem. Int. Ed.* **2012**, *51*, 8178.
(6) Yersin, H. *Highly Efficient OLEDs with Phosphorescent Materials*; Wiley-VCH: Weinheim, **2008**.
(7) (a) Bernards, D. A.; Slinker, J. D.; Malliaras, G. G.; Flores-Torres, S.; Abruna, H. D. *Appl. Phys. Lett.* **2004**, *84*, 4980; (b) Su, H.-C.; Wua, C.-C.; Fang, F.-C.; Wong, K.-T. *Appl. Phys. Lett.* **2006**, *89*, 261118.
(8) Tang, S.; Pan, J.; Buchholz, H. A.; Edman, L. *J Am Chem Soc* **2013**, *135*, 3647.
(9) Bernhard, S.; Barron, J. A.; Houston, P. L.; Abruña, H. D.; Ruglovsky, J. L.; Gao, X.; Malliaras, G. G. *J. Am. Chem. Soc.* **2002**, *124*, 13624.
(10) Zysman-Colman, E.; Slinker, J. D.; Parker, J. B.; Malliaras, G. G.; Bernhard, S. *Chem. Mater.* **2008**, *20*, 388.
(11) Schneider, G. E.; Bolink, H. J.; Constable, E. C.; Ertl, C. D.; Housecroft, C. E.; Pertegas, A.; Zampese, J. A.; Kanitz, A.; Kessler, F.; Meier, S. B. *Dalton Trans* **2014**, *43*, 1961.
(12) Slinker, J. D.; Bernards, D. A.; Houston, P. L.; Abruña, H. D.; Bernhard, S.; Malliaras, G. G. *Chem. Commun.* **2003**, *19*, 2392.
(13) Fernández-Hernández, J. M.; Ladouceur, S.; Shen, Y.; Iordache, A.; Wang, X.; Donato, L.; Gallagher-Duval, S.; de Anda Villa, M.; Slinker, J. D.; De Cola, L.; Zysman-Colman, E. *J. Mater. Chem. C* **2013**, *submitted*, Manuscript ID: TC.
(14) (a) Donato, L.; Abel, P.; Zysman-Colman, E. *Dalton Trans.* **2013**, *42*, 8402; (b) Fernandez-Hernandez, J. M.; Ladouceur, S.; Shen, Y.; Iordache, A.; Wang, X.; Donato, L.; Gallagher-Duval, S.; de Anda Villa, M.; Slinker, J. D.; De Cola, L.; Zysman-Colman, E. *J. Mater. Chem. C* **2013**, *1*, 7440; (c) Ladouceur, S.; Fortin, D.; Zysman-Colman, E. *Inorg. Chem.* **2011**, *50*, 11514; (d) Ladouceur, S.; Swanick, K. N.; Gallagher-Duval, S.; Ding, Z.; Zysman-Colman, E. *Eur. J. Inorg. Chem.* **2013**, *2013*, 5329.
(15) (a) He, L.; Duan, L.; Qiao, J.; Wang, R.; Wei, P.; Wang, L.; Qiu, Y. *Adv. Funct. Mater.* **2008**, *18*, 2123; (b) Mydlak, M.; Bizzarri, C.; Hartmann, D.; Sarfert, W.; Schmid, G.; De Cola, L. *Adv. Funct. Mater.* **2010**, *20*, 1812; (c) Kessler, F.; Costa, R. D.; Di Censo, D.; Scopelliti, R.; Ortí, E.; Bolink, H. J.; Meier, S.; Sarfert, W.; Gratzel, M.; Nazeeruddin, M. K.; Baranoff, E. *Dalton Trans.* **2012**, *41*, 180; (d) De Angelis, F.; Fantacci, S.; Evans, N.; Klein, C.; Zakeeruddin, S. M.; Moser, J.-E.; Kalyanasundaram, K.; Bolink, H. J.; Gratzel, M.; Nazeeruddin, M. K. *Inorg. Chem.* **2007**, *46*, 5989; (e) Yang, C.-H.; Beltran, J.; Lemaur, V.; Cornil, J.; Hartmann, D.; Sarfert, W.; Fröhlich, R.; Bizzarri, C.; De Cola, L. *Inorg. Chem.*

2010, *49*, 9891; (f) Darmawan, N.; Yang, C. H.; Mauro, M.; Raynal, M.; Heun, S.; Pan, J.; Buchholz, H.; Braunstein, P.; De Cola, L. *Inorg Chem* **2013**, *52*, 10756; (g) Monti, F.; Kessler, F.; Delgado, M.; Frey, J.; Bazzanini, F.; Accorsi, G.; Armaroli, N.; Bolink, H. J.; Orti, E.; Scopelliti, R.; Nazeeruddin, M. K.; Baranoff, E. *Inorg Chem* **2013**, *52*, 10292; (h) Chen, W.-T.; Chen, Y.-J.; Wu, C.-S.; Lin, J.-J.; Su, W.-L.; Chen, S.-H.; Wang, S.-P. *Inorg. Chim. Acta* **2013**, *408*, 225; (i) Chen, B.; Li, Y.; Yang, W.; Luo, W.; Wu, H. *Org. Electron.* **2011**, *12*, 766.
(16) (a) Murphy, L.; Congreve, A.; Palsson, L. O.; Williams, J. A. *Chem. Commun.* **2010**, *46*, 8743; (b) Wang, X.; Jia, J.; Huang, Z.; Zhou, M.; Fei, H. *Chem. Eur. J.* **2011**, *17*, 8028.
(17) Bao, Y.; Wang, H.; Li, Q.; Liu, B.; Li, Q.; Bai, W.; Jin, B.; Bai, R. *Macromolecules* **2012**, *45*, 3394.
(18) (a) Cui, Y.; Mo, H.-J.; Chen, J.-C.; Niu, Y.-L.; Zhong, Y.-R.; Zheng, K.-C.; Ye, B.-H. *Inorg. Chem.* **2007**, *46*, 6427; (b) Wenger, O. S. *Acc. Chem. Res.* **2013**, *46*, 1517; (c) Wenger, O. S. *Coord. Chem. Rev.* **2014**, DOI: 10.1016/j.ccr.2014.03.025.
(19) (a) Shan, G. G.; Li, H. B.; Sun, H. Z.; Cao, H. T.; Zhu, D. X.; Su, Z. M. *Dalton Trans* **2013**, *42*, 11056; (b) He, L.; Qiao, J.; Duan, L.; Dong, G.; Zhang, D.; Wang, L.; Qiu, Y. *Adv. Funct. Mater.* **2009**, *19*, 2950; (c) Sengottuvelan, N.; Seo, H.-J.; Kang, S.-K.; Kim, Y.-I. *Bull. Korean Chem. Soc.* **2010**, *31*, 2309; (d) Yun, S.-J.; Seo, H.-J.; Song, M.; Jin, S.-H.; Kim, Y. I. *Bull. Korean Chem. Soc.* **2012**, *33*, 3645.
(20) Slinker, J. D.; Gorodetsky, A. A.; Lowry, M. S.; Wang, J.; Parker, S. T.; Rohl, R.; Bernhard, S.; Malliaras, G. G. *J. Am. Chem. Soc.* **2004**, *126*, 2763.
(21) Freys, J. C.; Bernardinelli, G.; Wenger, O. S. *Chem. Commun.* **2008**, 4267.
(22) Sun, L.; Galan, A.; Ladouceur, S.; Slinker, J. D.; Zysman-Colman, E. *J. Mater. Chem.* **2011**, *21*, 18083.
(23) Vezzu, D. A.; Deaton, J. C.; Jones, J. S.; Bartolotti, L.; Harris, C. F.; Marchetti, A. P.; Kondakova, M.; Pike, R. D.; Huo, S. *Inorg Chem* **2010**, *49*, 5107.
(24) St-Pierre, G.; Ladouceur, S.; Fortin, D.; Zysman-Colman, E. *Dalton Trans.* **2011**, *40*, 11726.
(25) Campeau, L.-C.; Rousseaux, S.; Fagnou, K. *J. Am. Chem. Soc.* **2005**, *127*, 18020.
(26) Nonoyama, M. *Bull. Chem. Soc. Jpn.* **1974**, *47*, 767.
(27) (a) Thummel, R. P.; Goulle, V.; Chen, B. *J. Org. Chem.* **1989**, *54*, 3057; (b) Xiao, J.-C.; Shreeve, J. n. M. *J. Org. Chem.* **2005**, *70*, 3072.
(28) Phan, H. V.; Chakraborty, P.; Chen, M.; Calm, Y. M.; Kovnir, K.; Keniley, L. K., Jr.; Hoyt, J. M.; Knowles, E. S.; Besnard, C.; Meisel, M. W.; Hauser, A.; Achim, C.; Shatruk, M. *Chem. Eur. J.* **2012**, *18*, 15805.
(29) Laurila, E.; Oresmaa, L.; Niskanen, M.; Hirva, P.; Haukka, M. *Crystal Growth & Design* **2010**, *10*, 3775.
(30) Gutowsky, H. S.; Holm, C. H. *J. Chem. Phys.* **1956**, *25*, 1228.
(31) Pavlishchuk, V. V.; Addison, A. W. *Inorg. Chim. Acta* **2000**, *298*, 97.
(32) Cardona, C. M.; Li, W.; Kaifer, A. E.; Stockdale, D.; Bazan, G. C. *Adv. Mater.* **2011**, *23*, 2367.
(33) Melhuish, W. H. *J. Phys. Chem.* **1961**, *65*, 229.
(34) (a) Hohenberg, P.; Kohn, W. *Phys. Rev.* **1964**, *136*, B864; (b) Kohn , W.; Sham, L. J. *Phys. Rev.* **1965**, *140*, A1133; (c) In *The Challenge of d and f Electrons,*; Salahub, D. R., Zerner, M. C., Eds.; ACS: Washington, DC, **1989**; (d) Stratmann, R. E.; Scuseria, G. E.; Frisch, M. J. *J. Chem. Phys.* **1998**, *109*, 8218; (e) Bauernschmitt, R.; Ahlrichs, R. *Chem. Phys. Lett.* **1996**, *256*, 454; (f) Casida, M. E.; Jamorski, C.; Casida, K. C.; Salahub, D. R. *J. Chem. Phys.* **1998**, *108*, 4439.
(35) Frisch, M. J.; Trucks, G. W.; Schlegel, H. B.; Scuseria, G. E.; Robb, M. A.; Cheeseman, J. R.; Zakrzewski, V. G.; Montgomery, J. A.; Stratmann, R. E.; Burant, J. C.; Dapprich, S.;

J.M., M.; Daniels, A. D.; Kudin, K. N.; Strain, M. C.; Farkas, O.; Tomasi, J.; Barone, V.; Cossi, M.; Cammi, R.; Mennucci, B.; Pomelli, C.; Adamo, C.; Clifford, S.; Ochterski, J.; Peterson, G. A.; Ayala, P. Y.; Cui, Q.; Morokuma, K.; Malik, A.; Rabuck, A. D.; Raghavachari, K.; Foresman, J. B.; Cioslowski, J.; Ortiz, J. V.; Baboul, A. G.; Stefanov, B. B.; Liu, G.; Liashenko, A.; Piskorz, P.; Komaromi, I.; Gomperts, R.; Martin, R. L.; Challacombe, M.; Gill, P. M. W.; Johnson, B. G.; Chen, W.; Wong, M. W.; Andres, J. L.; Head-Gordon, M.; Replogle, E. S.; Pople, J. A. *Gaussian 98 (Revision A.6)*; Pittsburgh, PA, **1998**

(36) (a) Becke, A. D. *J. Chem. Phys.* **1993**, *98*, 5648; (b) Lee, C.; Yang, W.; Parr, R. G. *Phys. Rev. B* **1988**, *37*, 785; (c) Miehlich, B.; Savin, A.; Stoll, H.; Preuss, H. *Chem. Phys. Lett.* **1989**, *157*, 200.

(37) (a) Binkley, J. S.; Pople, J. A.; Hehre, W. J. *J. Am. Chem. Soc.* **1980**, *102*, 939; (b) Stevens, W. J.; Basch, W. J.; Krauss, M. *J. Chem. Phys.* **1984**, *81*, 6026; (c) Stevens, W. J.; Krauss, M.; Basch, H.; Jasien, P. G. *Can. J. Chem.* **1992**, *70*, 612; (d) Cundari, T. R.; Stevens, W. J. *J. Chem. Phys.* **1993**, *98*, 5555.

(38) (a) Gordon, M. S.; Binkley, J. S.; Pople, J. A.; Pietro, W. J.; Hehre, W. J. *J. Am. Chem. Soc.* **1982**, *104*, 2797; (b) Pietro, W. J.; Francl, M. M.; Hehre, W. J.; Defrees, D. J.; Pople, J. A.; Binkley, J. S. *J. Am. Chem. Soc.* **1982**, *104*, 5039; (c) Dobbs, K. D.; Hehre, W. J. *J. Comput. Chem.* **1986**, *7*, 359; (d) Dobbs, K. D.; Hehre, W. J. *J. Comput. Chem.* **1987**, *8*, 861; (e) Dobbs, K. D.; Hehre, W. J. *J. Comput. Chem.* **1987**, *8*, 880; (f) Ditchfield, R.; Hehre , W. J.; Pople, J. A. *J. Chem. Phys.* **1971**, *54*, 724; (g) Hehre, W. J.; Ditchfield, R.; Pople, J. A. *J. Chem. Phys.* **1972**, *56*, 2257; (h) Hariharan, P. C.; Pople, J. A. *Theor. Chim. Acta* **1973**, *28*, 213; (i) Hariharan, P. C.; Pople, J. A. *Mol. Phys.* **1974**, *27*, 209; (j) Gordon, M. S. *Chem. Phys. Lett.* **1980**, *76*, 163.

(39) Tomasi, J.; Mennucci, B.; Cammi, R. *Chem. Rev.* **2005**, *105*, 2999.

(40) You, Y.; Park, S. Y. *J. Am. Chem. Soc.* **2005**, *127*, 12438.

(41) Xiao, J.-C.; Shreeve, J. n. M. *J. Org. Chem.* **2005**, *70*, 3072.

(42) (a) Crosby, G. A.; Demas, J. N. *J. Phys. Chem.* **1971**, *75*, 991; (b) Fery-Forgues, S.; Lavabre, D. *J. Chem. Educ.* **1999**, *76*, 1260.

(43) Frisch, M. J.; Trucks, G. W.; Schlegel, H. B.; Scuseria, G. E.; Robb, M. A.; Cheeseman, J. R.; Scalmani, G.; Barone, V.; Mennucci, B.; Petersson, G. A.; Nakatsuji, H.; Caricato, M.; Li, X.; Hratchian, H. P.; Izmaylov, A. F.; Bloino, J.; Zheng, G.; Sonnenberg, J. L.; Hada, M.; Ehara, M.; Toyota, K.; Fukuda, R.; Hasegawa, J.; Ishida, M.; Nakajima, T.; Honda, Y.; Kitao, O.; Nakai, H.; Vreven, T.; Montgomery, J., J. A.; Peralta, J. E.; Ogliaro, F.; Bearpark, M.; Heyd, J. J.; Brothers, E.; Kudin, K. N.; Staroverov, V. N.; Kobayashi, R.; Normand, J.; Raghavachari, K.; Rendell, A.; Burant, J. C.; Iyengar, S. S.; Tomasi, J.; Cossi, M.; Rega, N.; Millam, J. M.; Klene, M.; Knox, J. E.; Cross, J. B.; Bakken, V.; Adamo, C.; Jaramillo, J.; Gomperts, R.; Stratmann, R. E.; Yazyev, O.; Austin, A. J.; Cammi, R.; Pomelli, C.; Ochterski, J. W.; Martin, R. L.; Morokuma, K.; Zakrzewski, V. G.; Voth, G. A.; Salvador, P.; Dannenberg, J. J.; Dapprich, S.; Daniels, A. D.; Farkas, Ö.; Foresman, J. B.; Ortiz, J. V.; Cioslowski, J.; Fox, D. J., 7.0 ed.; Wallingford, CT, **2009**

(44) (a) Hohenberg, P.; Kohn, W. *Phys. Rev.* **1964**, *B136*, 864; (b) Kohn, W.; Sham, L. *J. Phys. Rev.* **1965**, *A140*, 1133; (c) Parr, R. G.; Yang, W. *Density-functional theory of atoms and molecules*; Oxford Univ. Press: Oxford, **1989**.

(45) Becke, A. D. *J. Chem. Phys.* **1993**, *98*, 5648.

(46) Rassolov, V. A.; Pople, J. A.; Ratner, M. A.; Windus, T. L. *J. Chem. Phys.* **1998**, *109*, 1223.

(47) (a) Ladouceur, S.; Fortin, D.; Zysman-Colman, E. *Inorg. Chem.* **2010**, *49*, 5625; (b) Lowry, M. S.; Hudson, W. R.; Pascal Jr., R. A.; Bernhard, S. *J. Am. Chem. Soc.* **2004**, *126*, 14129.

(48) O'Boyle, N. M. *GaussSum 2.0* Dublin City University; Dubin Ireland, **2006**; *Available at* http://gausssum.sf.net.

TOC Graphic